Vietnam Journal of Earth Sciences, 45(1), 111-130, https://doi.org/10.15625/2615-9783/18021

Vietnam Journal of Earth Sciences
https://vjs.ac.vn/index.php/jse

Earthquake affects subsidence in Jakarta using Sentinel-1A time series images and 2D-MSBAS method

Mokhamad Yusup Nur Khakim[1*], Supardi Supardi[1], Takeshi Tsuji[2]

[1]*Department of Physics, Mathematics and Natural Science Faculty, Sriwijaya University, Indonesia*

[2]*University of Tokyo, 7-3-1 Hongo, Bunkyo-ku, Tokyo 113-8656, Japan*

Received 7 September 2022; Received in revised form 12 November 2022; Accepted 16 December 2022

ABSTRACT

Excessive groundwater extraction has been well known as the main factor causing land subsidence in several cities in Jakarta Basin, Indonesia. This area is surrounded by active geological structures and has thick sediments. This study emphasizes the impacts of earthquakes on subsidence over Jakarta and its surroundings by using the Sentinel-1A images and 2D-MSBAS (Multidimensional Small Baseline Subset) method. Sixty-one ascending and 66 descending Sentinel-1A images were utilized to derive 121 deformation maps from 26 March 2017 to 2 July 2019 by using the 2D-MSBAS method. Linear and nonlinear displacement variations were analyzed to understand earthquake impacts on the subsidence and their seasonal characteristics. On 23 January 2018, the *Mw* 5.9 earthquake shaking off the coast of Java significantly affected ground surface subsidence in Jakarta. A cumulative magnitude and linear rate increase of the subsidence reached approximately -196 mm and -44 mm/yr, respectively, during the period of this study. Besides the subsidence rate changes, the earthquake also affected the expansion of the localized subsiding areas at several sites. The earthquake-activated fault affected the ground surface of the surrounding area, moving east and subsiding in the western part of the study area. Meanwhile, variations of the nonlinear subsidence to the seasonal precipitation depended on the aquifer system behavior to retain an elastic expansion and land cover types in the investigated regions.

Keywords: Groundwater extraction; subsidence; earthquakes; Jakarta; Sentinel-1A; MSBAS.

1. Introduction

Jakarta is the capital city of Indonesia, with a population of about 10 million and a total area of 669 km^2 (Abidin et al., 2008). This city lies in the Jakarta Basin and continuously sinks due to the extensive groundwater extraction (Chaussard et al., 2013). Several studies have been conducted on land subsidence in Jakarta city with different methods and purposes. Magnitudes of cumulative subsidence in this area were up to 80 cm from 1982 to 1991 and up to 160 cm from 1991 to 1997 based on leveling surveys, while about 20 cm from 1997 to 1999 was measured using Global Positioning System (G.P.S.) survey methods (Abidin et al. 2001). The estimated subsidence rates were 1-10 cm/year between 1997 and 2005 from G.P.S. surveys (Abidin et al., 2008).

The G.P.S. measurements are limited to the spatial coverage. This limitation can be overcome by Interferometric Synthetic

*Corresponding author, Email: myusup_nkh@mipa.unsri.ac.id

Aperture Radar (InSAR) techniques with different SAR products to map spatial and temporal subsidence in the study area, such as JERS-1/SAR L-band data (Hirose et al., 2001), ALOS PALSAR (Abidin et al., 2011; Ng. et al., 2012; Tetuko et al., 2016), and terraSAR-X (Tetuko et al., 2016). These studies discussed factors causing land subsidence related to groundwater extraction, construction load, and soil consolidation. However, the impacts of earthquakes on the subsidence in Jakarta city have not been published yet. This city is located near a tectonically very active area. The primary earthquake sources are several active geological structures near this city, such as the Indo-Australia Subduction Zone, Cimandiri Fault, and Baribis Fault. The regional setting of this study area can be presented in Fig. 1. Active volcanoes surrounding this city are related to the subduction zone in which the Australian plate converges with the Eurasian plate with a convergence rate of 67 mm/yr (Sirait et al., 2020). This seismogenic structure is responsible for many earthquakes occurring in West Java.

Earthquakes varying in magnitude and hypocenter depth and their mechanisms are depicted by beach balls occurring from 2017 to 2019 around the study area, as shown in Fig. 1. Some beach balls are labeled to show the magnitude and date of the earthquake events. Two moderate-magnitude earthquakes occurred on 15 December 2017 and 23 January 2018. The M_w 6.5 earthquake struck off the coast of Java, West Java, on 15 December 2017, 230 km southeast of Jakarta city. This event occurred at a depth of 115 km with an oblique thrust fault mechanism, in which the strike of the fault plane is nearly perpendicular to the trench direction. The shaking of this M_w 6.5 earthquake was felt not only in Jakarta but also across West Java, Central Java, and Yogyakarta (Sirait et al., 2020). The intensity of shocks was felt in Jakarta city at IV Modified Mercalli Intensity (MMI). In addition, the M_w 5.9 earthquake struck off the coast of Java occurred on 23 January 2018 at 01:34:54 PM local time, 133 km southwest of Jakarta city, Indonesia (U.S. Geological Survey [USGS], 2020). This M_w 5.9 earthquake occurred at a depth of 46 km with an oblique thrust fault mechanism striking nearly parallel to the trench direction. This earthquake is categorized as a moderate magnitude and shallow event. The shaking was widely reported across Lampung, West Java, Central Java, and Jakarta in the maximum intensity scale IV-V MMI. The tremor in Jakarta was much stronger than in other recent earthquakes, damaging several houses.

Distant earthquakes could cause dynamic oscillation in an aquifer due to seismic waves. Many observation stations in Japan observed changes in crustal strains and groundwater conditions due to seismic waves associated with the 2004 earthquake off the west coast of northern Sumatra. The distances of these stations are more than 5000 km from the hypocenter (Kitagawa et al., 2006). Earthquakes induced more than 1-millimeter horizontal displacements in places up to 6000km from the epicenter (Fu and Sun, 2006). Such far-field deformation is an exciting study of how earthquakes affect subsidence over Jakarta City.

Therefore, this study aims to analyze earthquake impacts on spatial and temporal subsidence in the Jakarta Basin using Sentinel-1 images based on the 2D Multidimensional Small Baseline Subset (MSBAS) method (Sergey V. Samsonov and d'Oreye, 2017). In addition, seasonal displacements were analyzed to infer the behavior of the aquifer systems.

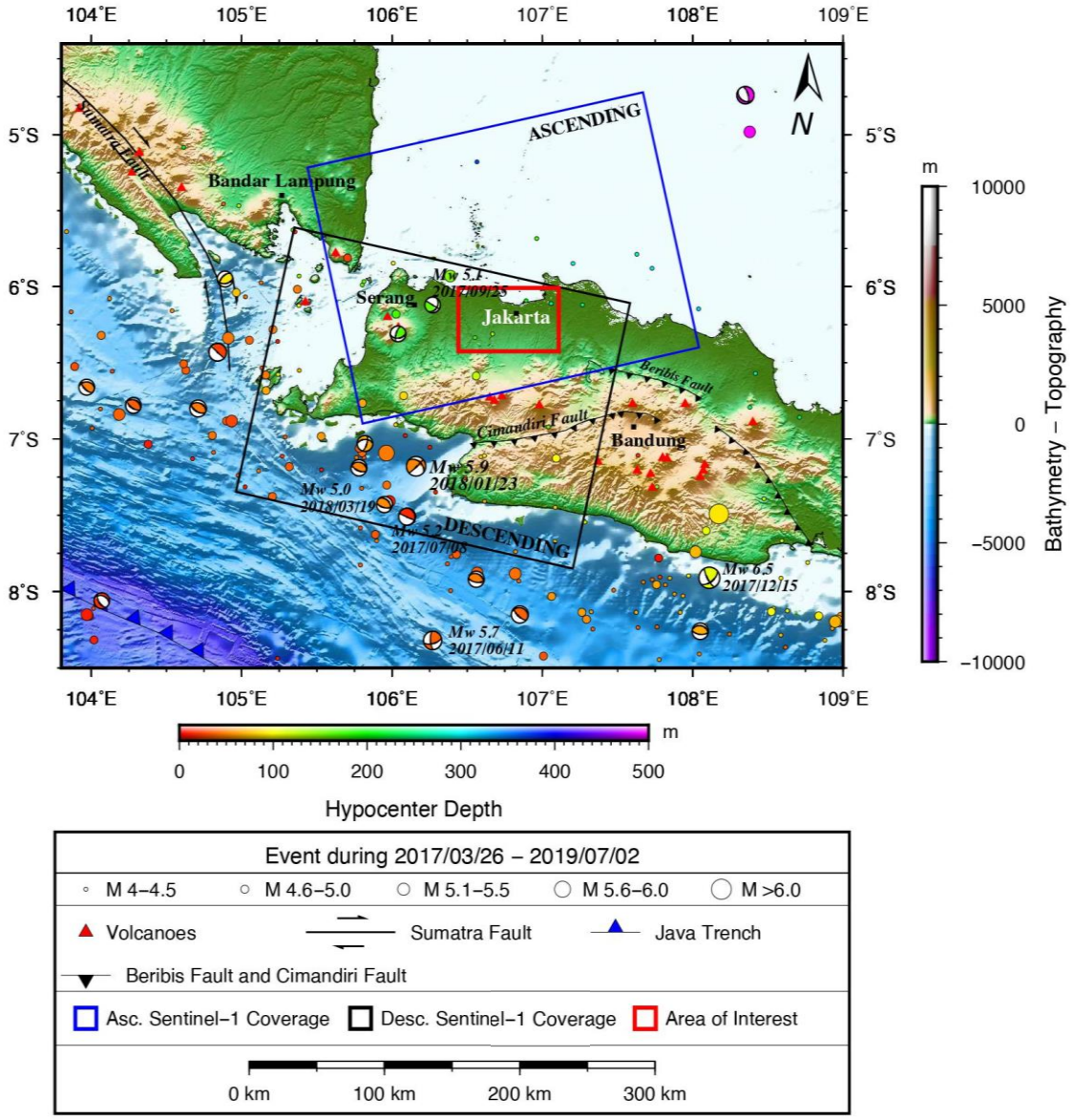

Figure 1. Geological structures and earthquake distribution in the study area from 26 March 2017 to 2 July 2019. Regional tectonic setting of the study area

2. Methods

2.1. Spatiotemporal deformation estimation

This study used the Sentinel-1A satellite mission dataset in the interferometric wide swath (IW) product using terrain observation by progressive scan (TOPS) because of its advantages over other products, such as short revisit time (12 days) covering a wide area and free access. Therefore, a time-series analysis based on this data is helpful for better spatial and temporal resolution of surface deformation monitoring (Yalvac, 2020). In this study, we utilized a total of 61 ascending (with

Path/Frame of 98/1160) and 66 descending (with Path/Frame of 47/614) Sentinel-1A Single Look Complex (SLC) images from 1 January 2017 to 30 July 2019. A flowchart of spatiotemporal deformation processing and analysis is presented in Fig. 2.

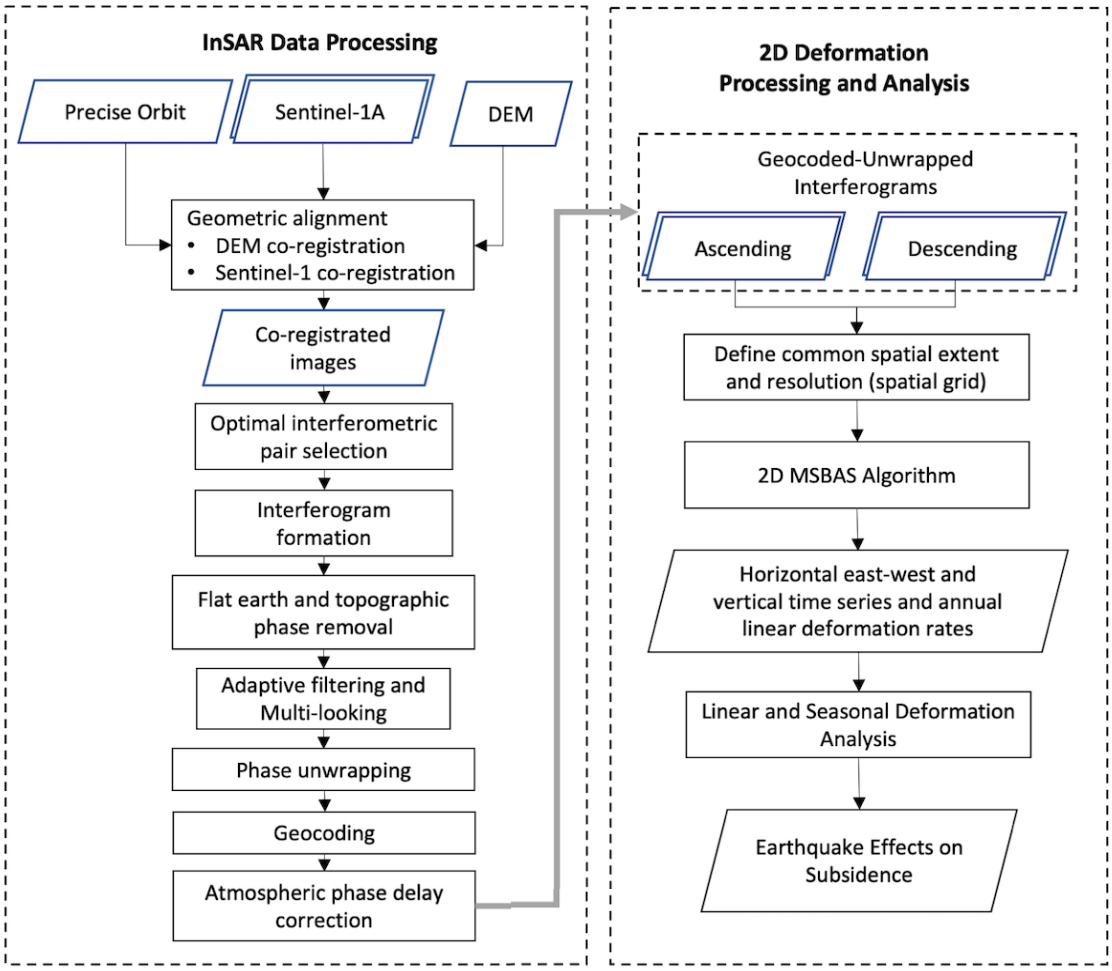

Figure 2. Flowchart of spatiotemporal deformation processing and analysis

SAR data processing has been performed using the GMTSAR software on the Ubuntu 18.04 platform (Sandwell et al., 2011; 2016). We concatenated bursts of sub-swath IW2 and sub-swath IW1-IW2 for ascending and descending images, respectively, to cover the study of interest. The slave images are aligned to a super master image (acquisition dates of 20180816 for ascending and 20180520 for descending) with geometrical alignment (Shirzaei et al., 2017; Xu et al., 2019). The geometric alignment of slave images to a super master image started with a pixel-wise estimate of range and azimuth offsets using precise orbits and a downsampled the 1-arcsecond shuttle radar topography mission (SRTM) digital elevation model (DEM), which covers the region of the SLC images (Xu et al., 2017). Each pixel in the DEM (longitude, latitude, ellipsoidal height) was back-projected into the range and azimuth coordinates of the master and slave images

using the precise orbit. The range and azimuth offsets were used to create a dense lookup map using a surfacing technique (Wessel and Smith, 1998). The slave images were deramped and demodulated (Miranda, 2015) before the slave images were resampled into the coordinates of the master image. We applied an enhanced spectral diversity (ESD) approach to remove burst discontinuities due to miss-registration along azimuth by refining the overall azimuth shift (Zhang et al., 2019).

The aligned SLC images were then selected to obtain the optimal interferometric pairs by calculating the spatial perpendicular and temporal baselines of the master and slave images. We selected the pairs with perpendicular baselines of less than 80 m and less than 100 m for descending and ascending pairs, respectively. In addition, the temporal baselines of less than 80 days and 100 days were selected for descending and ascending images, respectively. These perpendicular and temporal baseline networks are presented in Fig. 3. From the selection, 253 (ascending) and 223 (descending) interferometric pairs were able to be generated.

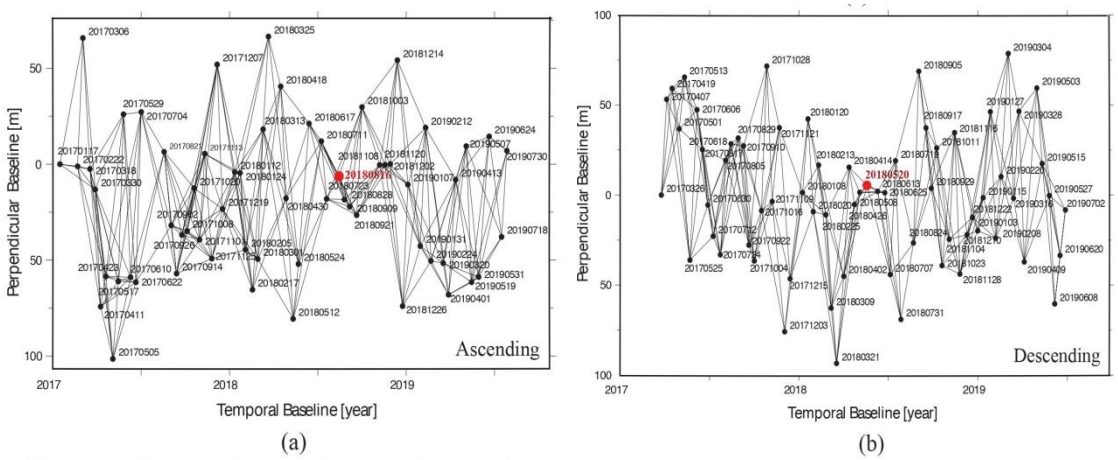

Figure 3. Perpendicular and temporal baseline networks to derive interferometric pairs. Red and black dots denote a supermaster and SAR images with the format of acquisition date [yyyymmdd], and gray lines indicate the interferogram pairs

In addition to the geometric alignment of images, the SRTM DEM removed the topographic phase from the observed interferometric phase. Furthermore, the phase term from noise was removed using Goldstein's filter and multi-looking (averaging 8 pixels in range and 2 pixels in azimuth). The interferogram was unwrapped using the Statistical-cost, Network-flow Algorithm for Phase Unwrapping (SNAPHU) with a coherence threshold of 0.2 (Chen and Zebker, 2001). After successfully unwrapping, the interferometric phase images were projected into a map coordinate system (WGS84). The interferometric atmospheric phase delay was removed using the Generic Atmospheric Correction Online Service (GACOS) for InSAR tropospheric delay maps.

Horizontal east-west and vertical time series consisting of 242 images were estimated from ascending and descending datasets simultaneously using the 2D MSBAS technique (Sergey Samsonov 2019; Sergey Samsonov and d'Oreye 2012). First, deformation velocities using Equation (1).

$$\begin{pmatrix} \hat{A} \\ \lambda L \end{pmatrix} \begin{pmatrix} V_E \\ V_U \end{pmatrix} = \begin{pmatrix} \widehat{\Phi} \\ 0 \end{pmatrix} \quad (1)$$

where matrix $\hat{A} = \{s_E\, A, s_U A\}$ consists of time intervals between consecutive SAR acquisitions A and east and up components of a line-of-sight vector $s = \{s_E, s_U\} = \{-\cos\theta \sin\phi, \cos\phi\}$, θ is azimuth, and ϕ is incidence angles, V_E and V_U represent unknown horizontal east-west and vertical velocities to be determined by applying the singular value decomposition (S.V.D.), $\widehat{\Phi}$ represents observed DInSAR data, geocoded and resampled to a common grid, λ is a regularization parameter, and L is a zero, first, or second-order difference operator. The first-order Tikhonov regularization with a value of 0.1 was chosen to produce reasonable solutions to ill-posed problems, which solutions either do not exist, are non-unique or unstable. The solution of the first-order regularization was computed by least square fitting data and minimizing the solution norm (Sergey V. Samsonov et al., 2017). The 2D surface deformation time series are then reconstructed using Equation (2).

$$d_{E,U}^{i+1} = d_{E,U}^{i} + V_{E,U}^{i} \Delta t^{i} \quad (2)$$

where $d_{E,U}^{i}$ is cumulative 2D deformations at the time t^i, and Δt^i is time intervals of consecutive ascending and descending acquisitions.

2.2. Analysis of earthquake impacts and seasonal subsidence

Based on the vertical and horizontal east-west deformation derived from the MSBAS method, we analyzed the spatial and temporal impacts of the earthquakes on the ground surface deformation. Spatiotemporal subsidence development was observed from maps of cumulative vertical displacements. Furthermore, tectonic movement over the study area was analyzed based on horizontal displacement maps. As an active fault has not been identified over the study area, the characteristics of deformation changes in the spatial and temporal deformation were used to understand how earthquakes and shaking can impact the studied area.

Furthermore, linear and nonlinear deformation time series trends were also used to analyze the earthquake impacts. These linear trends were used to analyze the linear rate changes inferred as earthquake impacts. A model of nonlinear subsidence was estimated using Equation (3) (Khakim et al., 2014).

$$y(t) = a_0 + \sum_{n=1}^{2} a_n\, cos(n\omega t) + b_n\, sin(n\omega t) \quad (3)$$

where a_0 is the model's shift from interferometric noise, a_n and b_n are the maximum seasonal amplitude for vertical displacement oscillations, t and ω are the displacement oscillation's time and angular frequency, respectively.

We assumed around 1-year periodicity for initial parameters for inversion in the seasonal analysis because the ground surface deformation (uplift and subsidence) should be related to the annual discharge and recharge processes cycles. An adjusted R-square and root mean squared errors (RMSE) are two statistical parameters used to evaluate the fit goodness of the model.

Time series of nonlinear deformation were compared to variations of monthly precipitation to understand their seasonal characteristics. The precipitation data were obtained from the European Center for Medium-Range Weather Forecast (ECMWF). In addition, we evaluate the accuracy of the land subsidence values obtained from the MSBAS analysis by comparing them with the G.P.S. measurements.

3. Results

3.1. Spatio-temporal variations of land subsidence and horizontal displacement

Figure 4 shows 32 of 121 cumulative subsidence maps from 26 March 2017 to 2 July 2019 derived from the MSBAS method. Eastward and upward are defined by positive displacements, and westward and downward are negative displacements. The vertical displacement maps are set in the same color scale from -196 to 0 mm for all the maps to demonstrate the historical subsidence variations more clearly in the period considered in this work. The spatial extent of the subsiding area and subsidence magnitudes varied with time and generally increased in the Northern part of Jakarta, West Jakarta, Tangerang, and Bekasi.

Figure 4 also shows subsidence gradually increased in several areas from 2017/03/26 to 2018/01/24. The land subsidence experienced a slight change in spatial distributions starting in 2017/06/18. This change may be induced by the 11 June 2017 M_w 5.7 earthquake at a 7 km focal depth. This earthquake occurred 238 km south of Jakarta city, and the shock intensity was felt in this city at IV MMI. The subsidence spatially spread out to several areas. Such subsidence patterns were also observed as impacts of two earthquakes, i.e., 8 July and 25 September 2017. The former struck off the Java coast, 165 km southwest of Jakarta, with a moment magnitude of M_w 5.2 and a depth of 8.5 km. This earthquake may be indicated as a factor of the subsidence spreading spatially toward the Depok region. Meanwhile, the latter occurred 59 km west of Jakarta at a depth of 150.1 km with a magnitude of M_w 5.1. An impact of this earthquake is subsidence more concentrated over the western part of Jakarta and west-north Jakarta, as observed in the map of 2017/09/26 in Fig. 4. The distribution pattern of land subsidence continued for several months, even though the giant earthquake with the magnitude of M_w 6.5 occurred 215 km southeast of Jakarta on 15 December 2017.

However, the M_w 5.9 earthquake off the coast of Java, 133 km southwest of Jakarta, on 23 January 2018 induced the most considerable changes in subsidence in North, West, and Central Jakarta compared to other earthquake events. These significant changes were observed in the subsidence map of 2018/01/24 (Fig. 4). The amount of land subsidence tended to decrease nearly three months after this event, especially in Central Jakarta.

Furthermore, an increase in subsidence due to the earthquake can also be shown on the 2018/03/21 map of Fig. 4. This indicates that the increase might be related to the M_w 5.0 earthquake at 48.6 km deep, 156 km southwest of Jakarta on 19 March 2018. This figure also shows that the amounts of subsidence in several areas continuously increased after this earthquake.

Moreover, Fig. 5 shows variations of spatial patterns of horizontal displacement. The arrow direction and length in this figure represent the directions and magnitudes of the horizontal displacements. These maps show that observed horizontal displacements dominantly moved toward the east.

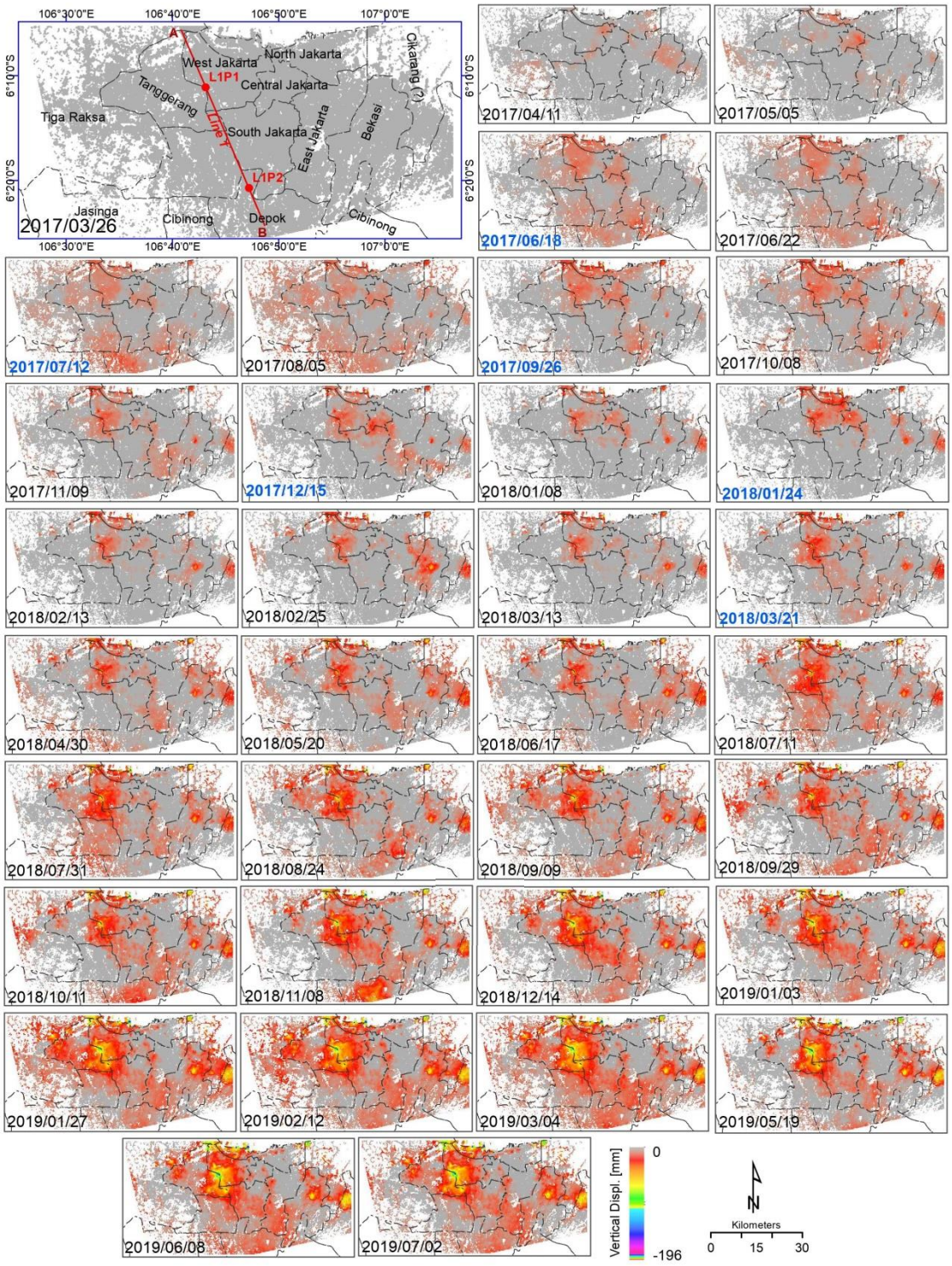

Figure 4. Selected maps of the cumulative subsidence time series over the study area estimated with MSBAS from 26 March 2017-2 July 2019

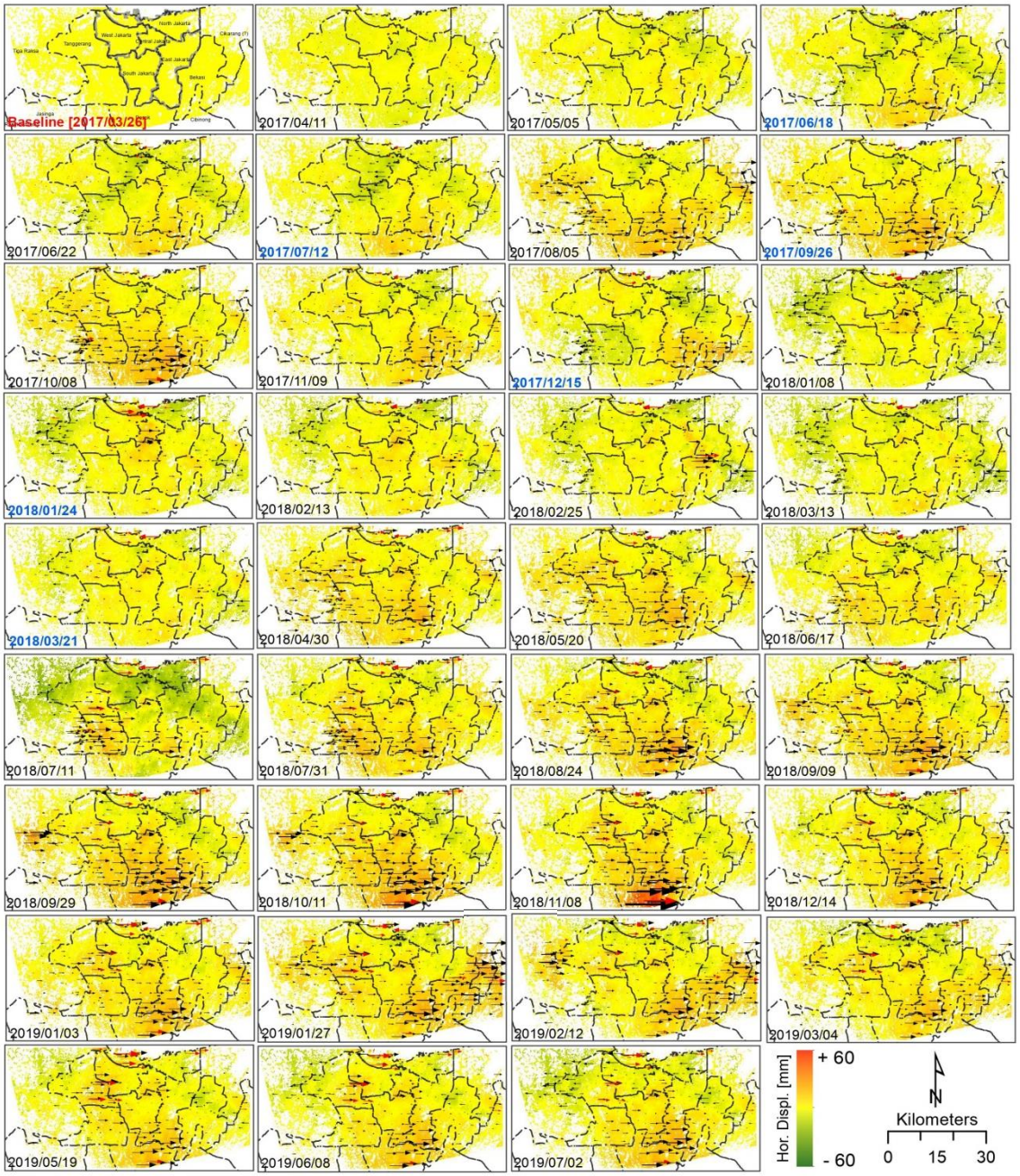

Figure 5. Cumulative horizontal east-west displacement time series for 35 epochs derived from the MSBAS method from 26 March 2017 to 2 July 2019

3.2. Deformation rates for the cumulative period of 26 March 2017 to 2 July 2019

In addition to the deformation time series, MSBAS processing also provides information on rates of ground surface deformations. The deformation rates varied spatially over the study area. Subsidence bowls were concentrated in several locations (i.e., P1-P16) as presented in Fig. 6a. The subsidence rate reached 54.95mm/yr at P1, 44 mm/yr at P6, and 68 mm/yr at P8

during the study period with the standard deviation as in Fig. 6b. A significant subsidence rate was also identified over other areas, such as Tangerang, Bekasi, and Tambun. On the other hand, lower magnitudes of subsidence occurred at P3, although this site is located near P1 and P2. Such a low subsidence rate also occurred at P13.

In addition, the rate of east-west horizontal displacement reached 30 mm/yr, as shown in Fig. 6c, with the standard deviation as in Fig. 6d. Patterns of the horizontal displacement in the southwest part of the map are associated with an indicative fault, namely Cisadane Fault. Furthermore, maps of aquifer zones (Fig. 6e-f) were used to identify the relation between subsidence distribution and aquifer conditions. This zonation was classified by the percentages of its area with groundwater declines into zones labeled damage, critical, prone, and safe, defined as more than 80%, 60-80%, 40-60%, and less than 40%, respectively. The more extensive subsidence occurred in areas associated with a prone zone. Meanwhile, places related to critical and damaged aquifers relatively more minor subsided compared to the prone site.

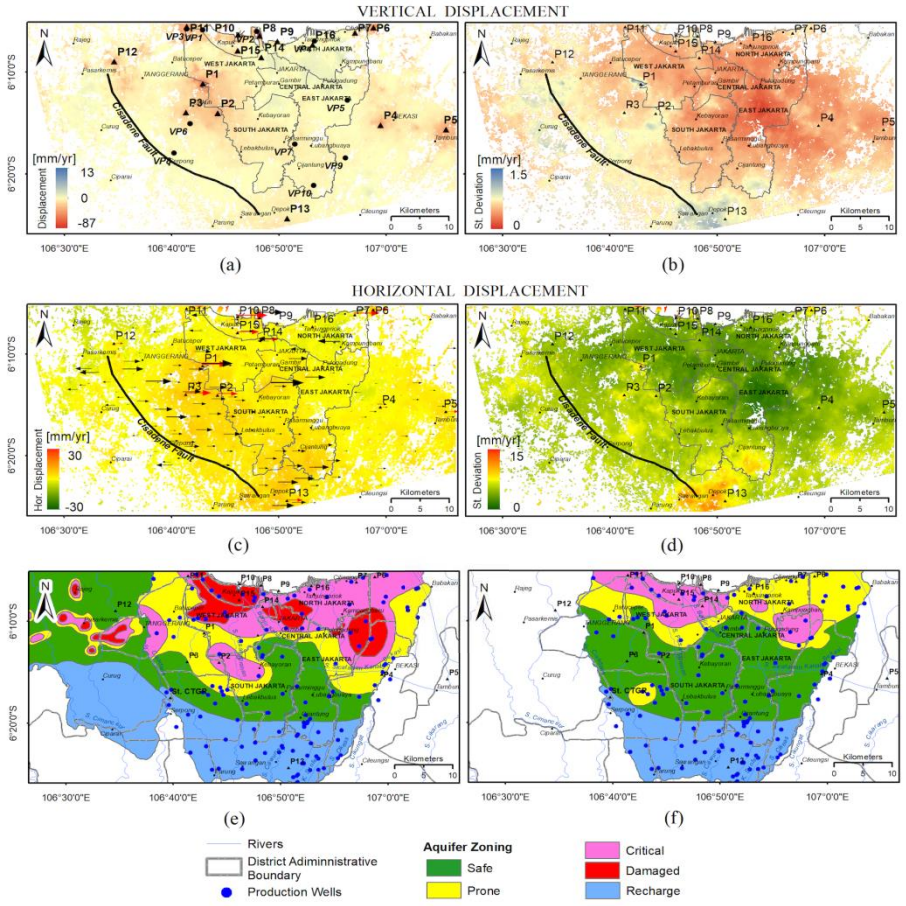

Figure 6. (a) Rate, (b) standard deviation of vertical displacements, (c) rate, (d) standard deviation of horizontal displacements measured using the MSBAS method from 26 March 2017 to 2 July 2019. Aquifer zones in depths of (d) 40-140 m, and (e) 140-250 m overlaid with a distribution of groundwater production wells. VP1-10 are points for subsidence validation. Aquifer zones are classified into damage, critical, prone, and safe, which are the percentages of its area with groundwater declines defined as more than 80%, 60-80%, 40-60%, and less than 40%, respectively

For verification, the subsidence rate derived from the MSBAS analysis was correlated to G.P.S. measurements provided by Geological Agency, Ministry of Energy and Mineral Resources. Ten points of G.P.S. stations, namely VP1-VP10, were utilized for the validation, as presented in Fig. 6a. The estimated rates of the subsidence from the MSBAS analysis are well-correlated with those of G.P.S. measurements with a correlation value of 0.95, as presented in Fig. 7.

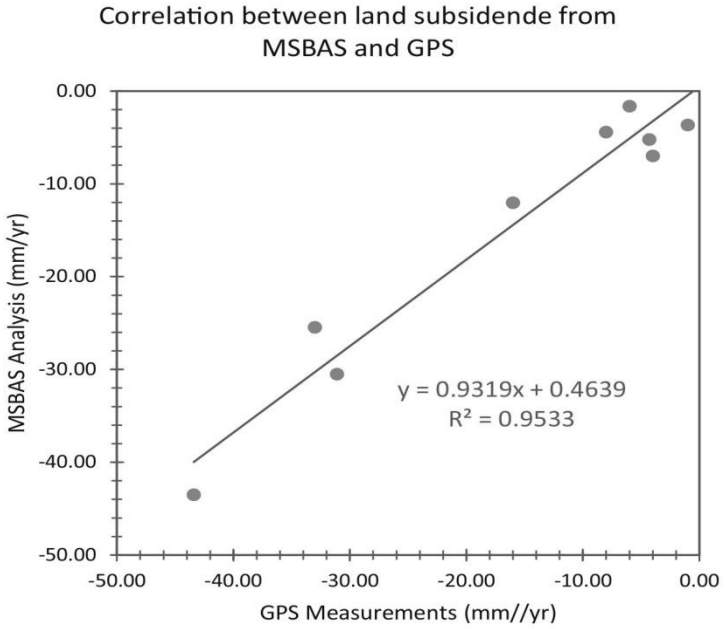

Figure 7. Correlation between subsidence from MSBAS analysis and G.P.S. measurements at 10 points (VP1-10 in Fig. 6a)

Although we do not have more detailed deformation data from G.P.S. measurements which is a limitation of this study, the MSBAS method has proven to be a method that has good accuracy for several applications, such as monitoring fast land surface subsidence in southern Saskatchewan (Canada) (S.V. Samsonov et al., 2014), mapping ground deformation at the Piton de la Fournaise volcano (Sergey V. Samsonov et al., 2017), measuring earthquake-related deformations in Iran (Yang et al., 2019), mapping. In addition, the previous studies on Jakarta's subsidence can provide an overview of the resulting subsidence for different time intervals (Chaussard et al., 2013; Hakim et al., 2020; Ng. et al., 2012). These studies show similar patterns and spatial extent of the subsiding areas to our results.

3.3. Time-series displacements for the cumulative period of 26 March 2017 to 2 July 2019

To understand the characteristics of vertical displacements in more detail, we create profiles of the time series along line A.B. (Fig. 4**)** across two points, L1P1 and L1P2, with large and small subsidence, respectively. Vertical displacement profiles along this line and the time series of the vertical displacements at these two points are shown in Fig. 8. According to the shapes, the most significant subsidence was at point L1P1. The land surface continuously moved downward,

reaching approximately -35 mm (Fig. 8a) and -120 mm (Fig. 8b) before and after 23 January 2018, respectively. On the other hand, oscillations of up-down movement approximately from -10 to 20 mm took place around point L1P2.

Furthermore, subsidence time series at L1P1 and L1P2 were cumulatively evaluated to analyze subsidence trends from 26 March 2017 to 2 July 2019. The results show a linear rate of the subsidence increased up to 31.69 mm/yr after the 23 January 2018 earthquakes (Fig. 8c). Meanwhile, the linear subsidence rate at L1P2 has a different trend from point L1P1 (Fig. 8d). The ground surface at this site instantaneously uplifted following the 23 January 2018 earthquake. Then, the displacement decreased sharply, as observed from this time series. Such changes in the linear subsidence rates at several points marked from the time series can also be presented in Fig. 9. We revealed deformation induced by an earthquake in the wrapped phase map using an individual interferometric pair of 20180112-20180124, as shown in Fig. 10a. Significant deformations occurred in the northern part of this study area, dominated by alluvium and floodplain coastal as geological conditions (Fig. 10b).

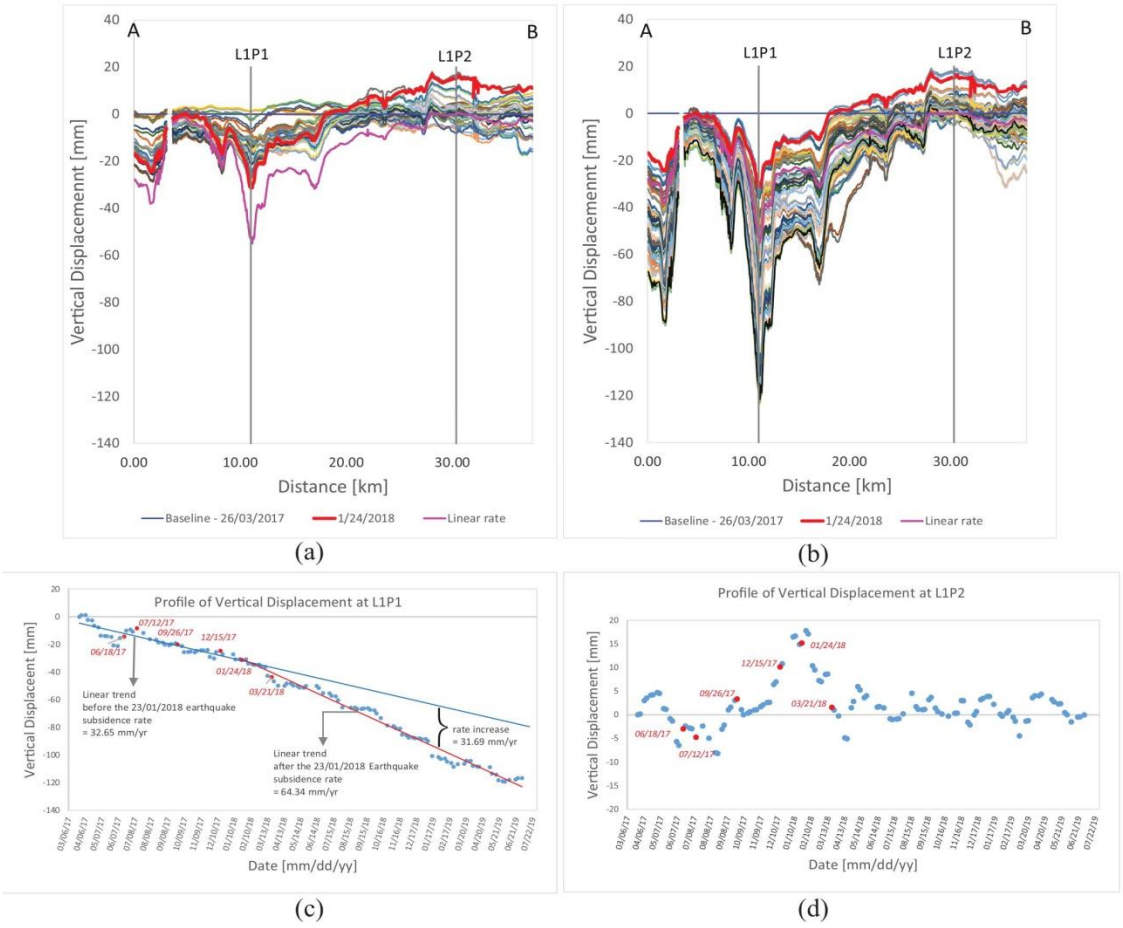

Figure 8. Time-series profiles of vertical displacements along line A.B. and a linear rate: (a) before; and (b) after the 23 January 2018 Earthquake; (c) time series of vertical displacement at point L1P1; and (d) at point L1P2

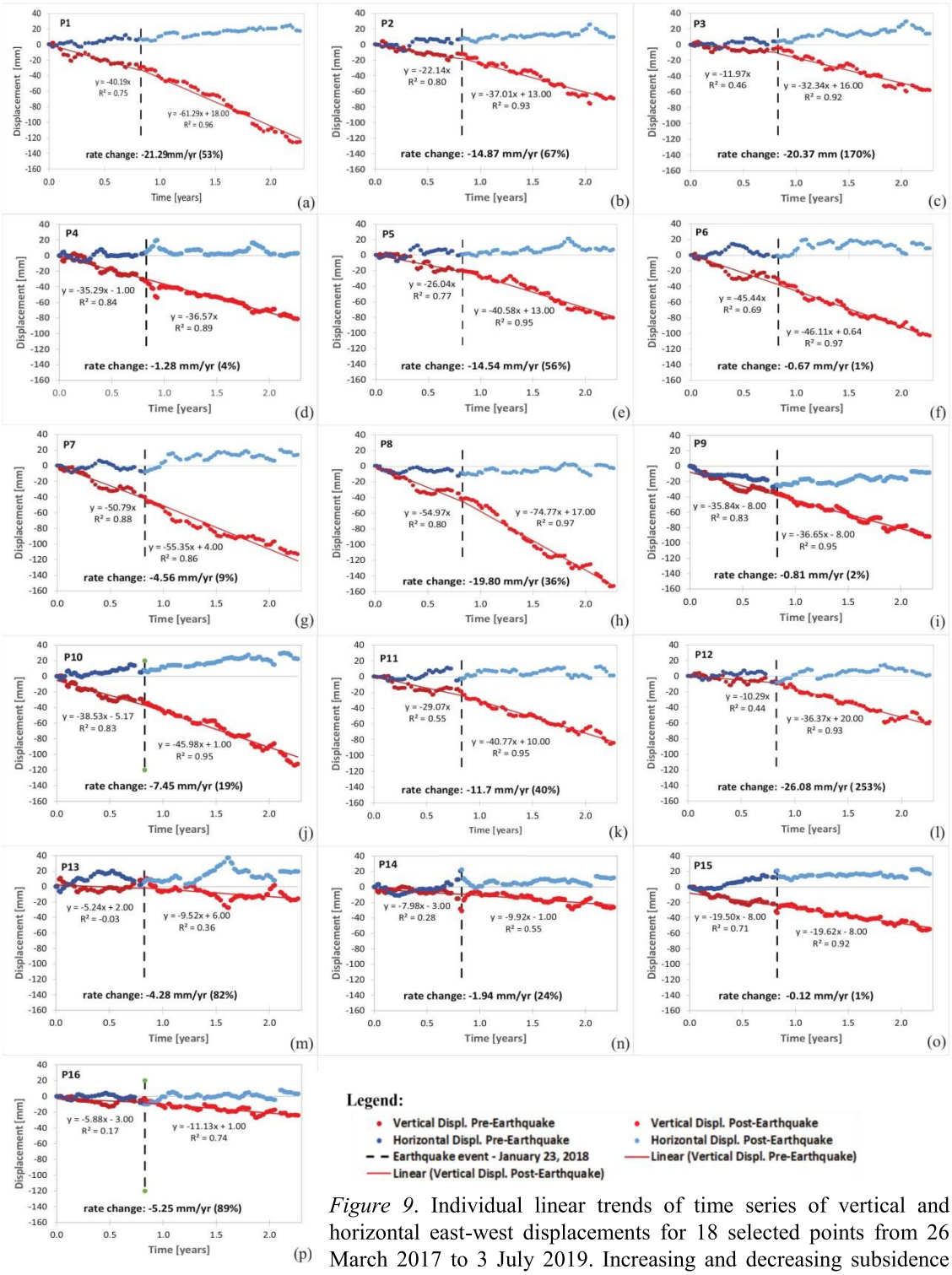

Figure 9. Individual linear trends of time series of vertical and horizontal east-west displacements for 18 selected points from 26 March 2017 to 3 July 2019. Increasing and decreasing subsidence rates are defined as positive and negative signs, respectively

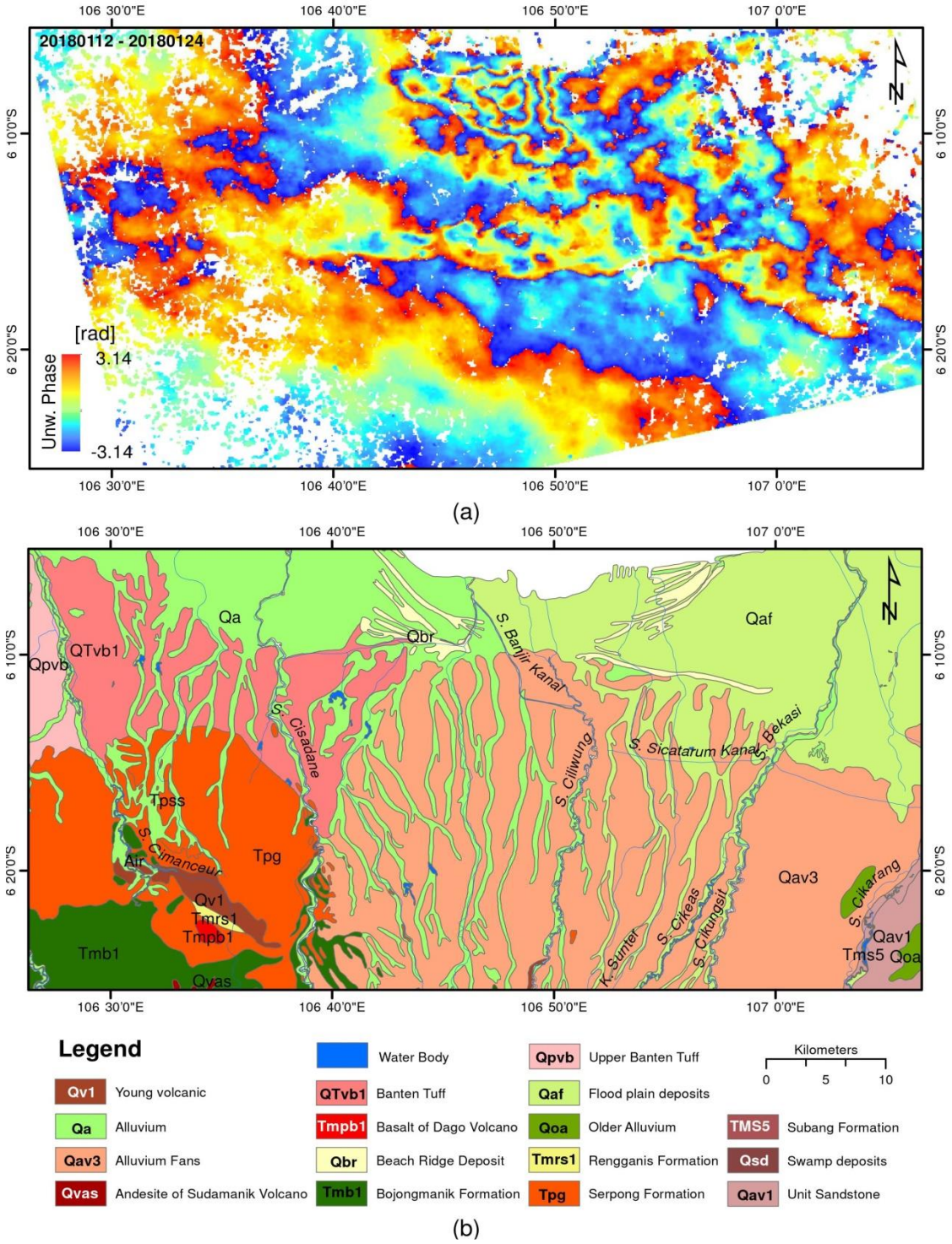

Figure 10. (a) Wrapped phase associated with the 5.9 M_w earthquake on 23 January 2018 was observed using a Sentinel-1 interferometric pair of 12-24 January 2018, and (b) a geological map of the area of interest

3.4. Nonlinear vertical displacements

A cumulative deformation consists of linear and nonlinear components as well as noises. The nonlinear vertical displacement is essential to understand the characteristics of the aquifer system response to seasonal variations. In general, the time series trends of the nonlinear component were related to variations of the precipitation over the study area, as shown in Fig. 11. However, variations of the nonlinear subsidence in several places, such as P3, P4, and P12, are less correlated with the precipitation variations. In addition, time lags between nonlinear subsidence and precipitation occurred in several locations, such as P14 and P15.

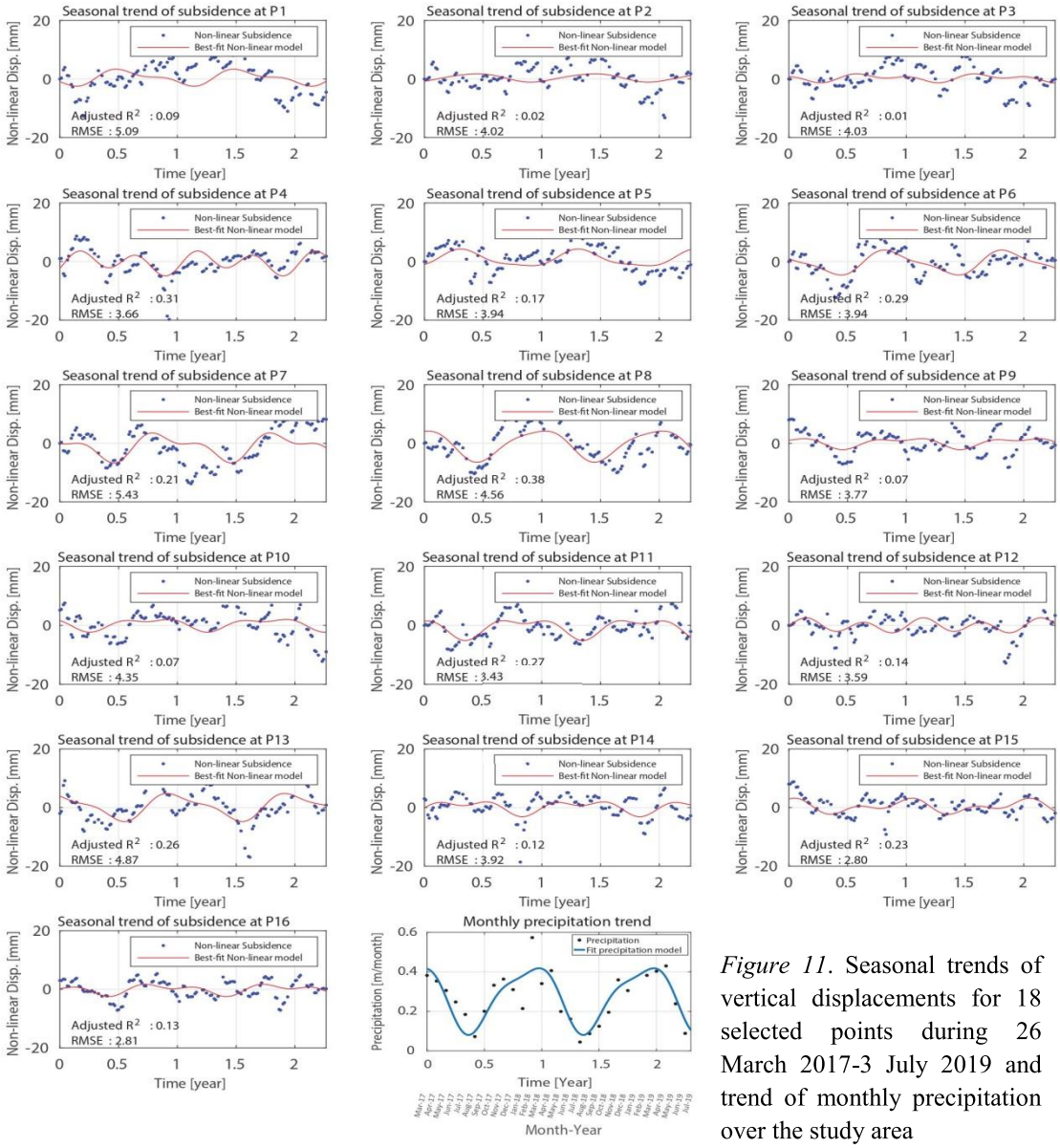

Figure 11. Seasonal trends of vertical displacements for 18 selected points during 26 March 2017-3 July 2019 and trend of monthly precipitation over the study area

4. Discussions

Extensive groundwater extraction has been well known as the main factor of the ground surface subsidence in several cities in the Jakarta Basin. Subsidence due to excessive groundwater withdrawal in Jakarta was investigated by other studies (Abidin et al., 2001; 2008; 2011; Delinom et al., 2009; Hakim et al., 2020; Ng. et al., 2012). Due to the study area being relatively near active geological structures, it is vulnerable to earthquake shaking from the surrounding areas. Therefore, we investigated earthquakes' impacts on land subsidence.

Due to the earthquake of 23 January 2018 most significantly affecting the subsidence than other earthquakes over the study area, we thus evaluated the linear rate changes by separating SAR datasets in MSBAS processing into two periods, i.e., before and after this earthquake. Therefore, the rate changes can be more easily mapped from linear rates of the before and aftershocks over the study area. Moreover, we assumed that other factors, such as groundwater extraction, construction load, and soil consolidation, inducing the subsidence rate remained constant during the study period. Thus, an increase in the subsidence rates in the study area was caused by earthquakes.

The results show that this earthquake significantly impacted subsidence's spatial extent, magnitude, and rate. Nearly circular patterns of subsidence were observed around points P1-P6 (Fig. 12(a),(b)). Subsidence rates after the earthquakes were commonly larger than those before the event in several areas, with a maximum change of -44 mm/yr, as presented in the top row of Fig.12. In addition, remarkable increases in the subsidence rate mainly occurred near the boundary between Tangerang and West Jakarta (P1, P2, P3, and P12) and partly in North Jakarta (P8). These areas experienced subsidence with rate increases from -15 mm/yr to -35 mm/yr. Besides the subsidence rate changes, the earthquake also caused the expansion of the subsiding area. A vast spatial expansion of the subsiding area was also observed around the Cisadane Fault and the surrounding area in the western study area, as shown in Fig. 12(c).

Although this earthquake was relatively far from Jakarta (~133 km), this event is indicated considerably affecting the subsidence over this city. We infer that soft soils amplified the shock over Jakarta during earthquakes, even the epicenter in the far field. During earthquakes, seismic amplification is potentially caused by low seismic velocities and the thick basin beneath the city (Saygin et al., 2016). Earthquake shaking decreased pore volume and thus raised pore pressure in alluvial fans (Wang et al. 2001). Consequently, more extensive subsidence occurred in several areas, including North Jakarta, West Jakarta, Bekasi, Tangerang, and Tambun. These areas are dominated by alluvium and coastal floodplain with a lithological composition of tuffaceous clay, sandy to gravelly clay, and sand interlayers. The aquifers consist of sandstone multilayers with a thickness of 3-18 m, transmissivities of 120-260 m^2/day, and a depth of wells between 140-250 m below the ground surface (Murtianto 1993). On the other hand, areas with lower subsidence, such as Lebak Bulus, Cijantung, and Depok, are lithologically dominated by tuff, pumice tuff, and tuffaceous sandstone with lower permeability and transmissivity of aquifers.

Fig. 12(c),(d) show east-west horizontal displacements before and after the earthquakes calculated separately using the MSBAS method. Greater eastward displacements are commonly occurred in areas experiencing significant subsidences. In general, horizontal displacements, initially toward the west direction before earthquakes, changed toward the east direction after the earthquakes. These direction changes are mainly in the Cisadane fault and surrounding areas in the western part of the study area (Fig. 12(f)). Thus, we indicated that the fault type might be a normal

fault formed by extensional forces, and consequently, the subsidence rate developed. Such a trend of extension in this area was consistent with the results of other studies based on G.P.S. measurements (Gunawan and Widiyantoro, 2019; Koulali et al., 2017).

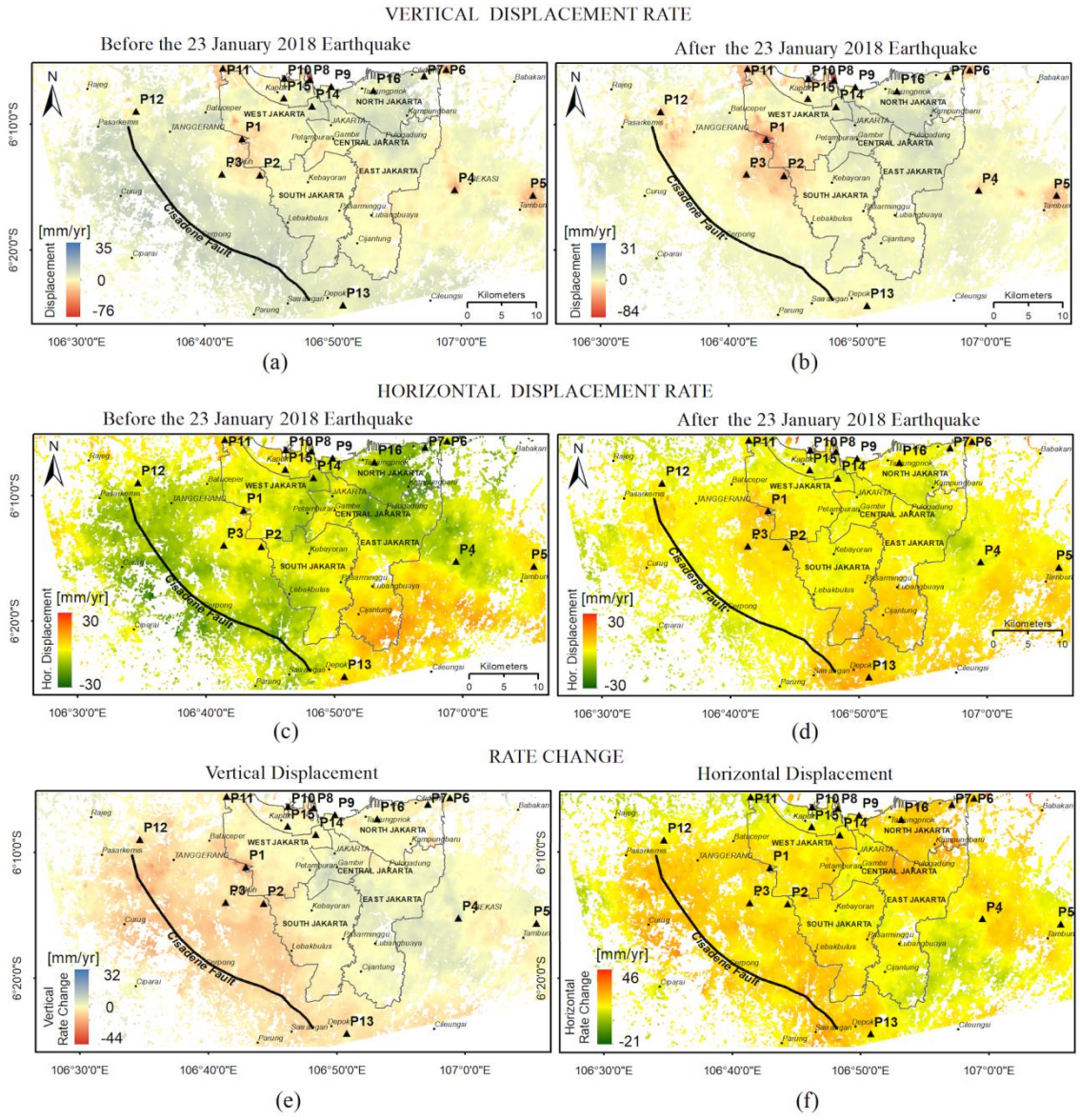

Figure 12. Maps of vertical and horizontal displacement rates before and after the earthquake and the rate changes

Seasonal subsidences were generally correlated with the precipitation. Thus, the aquifers can retain an elastic expansion to store groundwater from recharging, especially surface water. This elastic expansion compensated residual compaction in the aquifer system during the rainy season. In contrast, the seasonal trends were less

correlated with the precipitation variations in locations dominated by tuff, pumice tuff, and tuffaceous sandstone with lower permeability and transmissivity of aquifers. Thus, the nonlinear subsidence in these areas oscillated smaller amplitudes than in other areas. In addition, higher frequencies of the subsidence oscillations might be influenced by seepages of the precipitation and irrigation from rivers into the soil near the surface.

In addition, time lags between seasonal subsidence and precipitation were observed in several site locations of Jakarta city (P14, P15). Such lags between nonlinear karst subsidence and precipitation trends were also observed in Qingling-Jiangdi, China (Shi et al., 2021). They might be caused by the types of land covers in the study area, such as highways, pavements, dense buildings, and other infrastructure construction, covering soil layers and preventing precipitation seepages to the aquifers. In addition, these locations are associated with a zone of the damaged aquifer, which is compacted. Therefore, the oscillation amplitudes of the nonlinear subsidence were small. These locations also indicate experiencing lower cumulative subsidences and decreasing subsidence rate changes. Moreover, the groundwater extraction from the aquifer in these areas had been restricted under government regulation.

5. Conclusions

The MSBAS method has been successfully applied to reveal the impacts of earthquakes on ground surface subsidence. The Mw 5.9 earthquake shaking off the coast of Java shook Jakarta on 23 January 2018 and had more significant implications than any other earthquakes during the study period.

The earthquake shaking decreased pore volume and thus raised pore pressure in the alluvial fan. Consequently, it led to increases in the subsidence of the ground surface. Significant subsidences cumulatively reached approximately -196 mm with a maximum change in rates of -44 mm/yr in Tangerang, West Jakarta, and North Jakarta. Besides the subsidence rate changes, the earthquake also caused the expansion of the subsiding area in the western part of the study area, especially surrounding the Cisadane Fault.

Moreover, the time series of the nonlinear displacements in areas associated with alluvium deposits and coastal floodplains are generally related to seasonal precipitation but not in regions dominated by tuff, pumice tuff, and tuffaceous sandstone. The nonlinear subsidence in these areas oscillated smaller amplitudes than in other areas. In addition, higher frequencies of the subsidence oscillations might be influenced by seepages of the precipitation and irrigation from rivers into the soil near the surface. Time lags between nonlinear subsidence and rain might be caused by infrastructure constructions covering soil layers and preventing precipitation seepages to the aquifers. These areas also experienced lower cumulative surface depression and decreased subsidence rate changes.

Acknowledgments

We thank Sriwijaya University, Indonesia, for financial support through "*Penelitian Unggulan Kompetitif*," No: 0685/UN9/SK. B.U.K. K.P./2020, Geological Agency, Ministry of Energy and Mineral Resources, Republic of Indonesia for providing the data, and the European Space Agency (E.S.A.) for providing Sentinel-1 data. We thank the two anonymous reviewers and the academic editor for their constructive comments that helped to improve the paper.

References

Abidin H.Z., Andreas H., Djaja R., Darmawan D., Gamal M., 2008. Land subsidence characteristics of Jakarta between 1997 and 2005, as estimated using G.P.S. surveys. G.P.S. Solut., 12, 23-32. https://doi.org/10.1007/s10291-007-0061-0

Abidin H.Z., Andreas H., Gumilar I., Fukuda Y., Pohan Y.E., Deguchi T., 2011. Land subsidence of Jakarta (Indonesia) and its relation with urban development. Nat. Hazards, 59, 1753-1771. https://doi.org/10.1007/s11069-011-9866-9.

Abidin H.Z., Djaja R., Darmawan D., Hadi S., Akbar A., Rajiyowiryono H., Sudibyo Y., Meilano I., Kasuma M.A., Kahar J., Subarya C., 2001. Land subsidence of Jakarta (Indonesia) and its geodetic monitoring system. Nat. Hazards, 23, 365-387. https://doi.org/10.1023/A:1011144602064.

Chaussard E., Amelung F., Abidin H., Hong S., 2013. Remote Sensing of Environment Sinking cities in Indonesia : ALOS PALSAR detects rapid subsidence due to groundwater and gas extraction. Remote Sens. Environ., 128, 150-161. https://doi.org/10.1016/j.rse.2012.10.015.

Chen C.W., Zebker H.A., 2001. Two-dimensional phase unwrapping with use of Statistical Models for Cost Functions in Nonlinear Optimization. J. Opt. Soc. Am. A, 18, 338-351.

Delinom R.M., Assegaf A., Abidin H.Z., Taniguchi M., Suherman D., Lubis R.F., Yulianto E., 2009. The contribution of human activities to subsurface environment degradation in Greater Jakarta Area, Indonesia. Sci. Total Environ., 407, 3129-3141. https://doi.org/10.1016/j.scitotenv.2008.10.003

Fu G., Sun W., 2006. Global co-seismic displacements caused by the 2004 Sumatra-Andaman earthquake (Mw 9.1). Earth, Planets Sp., 58, 149-152. https://doi.org/10.1186/BF03353371.

Gunawan E., Widiyantoro S., 2019. Active tectonic deformation in Java, Indonesia inferred from a GPS-derived strain rate. J. Geodyn., 123, 49-54. https://doi.org/10.1016/j.jog.2019.01.004.

Hakim W.L., Achmad A.R., Lee C.W., 2020. Land subsidence susceptibility mapping in jakarta using functional and meta-ensemble machine learning algorithm based on time-series insar data. Remote Sens., 12, 1-26. https://doi.org/10.3390/rs12213627.

Hirose K., Maruyama Y., Murdohardono D., Effendi A., Abidin H.Z., 2001. Land subsidence detection using JERS-1 SAR Interferometry. Pap. Present. 22nd Asian Conf. Remote Sens., 6.

Khakim M.Y.N., Tsuji T., Matsuoka T., 2014. Lithology-controlled subsidence and seasonal aquifer response in the Bandung basin, Indonesia, observed by synthetic aperture radar interferometry. Int. J. Appl. Earth Obs. Geoinf., 32, 199-207. https://doi.org/10.1016/j.jag.2014.04.012.

Kitagawa Y., Koizumi N., Takahashi M., Matsumoto N., Sato T., 2006. Changes in groundwater levels or pressures associated with the 2004 earthquake off the west coast of northern Sumatra (M9.0). Earth, Planets Sp., 58, 173-179. https://doi.org/10.1186/BF03353375.

Koulali A., McClusky S., Susilo S., Leonard Y., Cummins P., Tregoning P., Meilano I., Efendi J., Wijanarto A.B., 2017. The kinematics of crustal deformation in Java from G.P.S. observations: Implications for fault slip partitioning. Earth Planet. Sci. Lett., 458, 69-79. https://doi.org/10.1016/j.epsl.2016.10.039.

Miranda N., 2015. Impact of the Elevation Antenna Pattern Phase Compensation on the Interferometric Phase Preservation. E.S.A. Tech. Note, 1-15. https://doi.org/ESA-EOPG-CSCOP-TN-0004.

Murtianto E., 1993. Hydrogeological Map of Indonesia, Sheet Jakarta Scale 1 :100,000. Bandung [Indonesia].

Ng A.H.M., Ge L., Li X., Abidin H.Z., Andreas H., Zhang K., 2012. Mapping land subsidence in Jakarta, Indonesia using persistent scatterer interferometry (P.S.I.) technique with ALOS PALSAR. Int. J. Appl. Earth Obs. Geoinf., 18, 232-242. https://doi.org/10.1016/j.jag.2012.01.018.

Samsonov, S., 2019. Three-dimensional deformation time series of glacier motion from multiple-aperture DInSAR observation. J. Geod. 93, 2651-2660. https://doi.org/10.1007/s00190-019-01325-y.

Samsonov S., d'Oreye N., 2012. Multidimensional time-series analysis of ground deformation from multiple InSAR data sets applied to Virunga Volcanic Province. Geophys. J. Int., 191, 1095-1108. https://doi.org/10.1111/j.1365-246X.2012.05669.x.

Samsonov S.V., d'Oreye N., 2017. Multidimensional Small Baseline Subset (MSBAS) for Two-Dimensional Deformation Analysis: Case Study Mexico City. Can. J. Remote Sens., 43, 318-329.

https://doi.org/10.1080/07038992.2017.1344926.

Samsonov S.V., Feng W., Peltier A., Geirsson H., d'Oreye N., Tiampo K.F., 2017. Multidimensional Small Baseline Subset (MSBAS) for volcano monitoring in two dimensions: Opportunities and challenges. Case study Piton de la Fournaise volcano. J. Volcanol. Geotherm. Res., 344, 121-138. https://doi.org/10.1016/j.jvolgeores.2017.04.017.

Samsonov S.V., González P.J., Tiampo K.F., D'Oreye N., 2014. Modeling of fast ground subsidence observed in southern Saskatchewan (Canada) during 2008-2011. Nat. Hazards Earth Syst. Sci., 14, 247-257. https://doi.org/10.5194/nhess-14-247-2014.

Sandwell D., Mellors R., Tong X., Wei M., Wessel P., 2011. Open Radar Interferometry Software for Mapping Surface Deformation. Eos, Trans. Am. Geophys. Union, 92, 234-235.

Sandwell D., Mellors R., Tong X., Xu X., Wei M., Wessel P., 2016. GMTSAR : An InSAR Processing System Based on Generic MApping Tools.

Saygin E., Cummins P.R., Cipta A., Hawkins R., Pandhu R., Murjaya J., Masturyono, Irsyam M., Widiyantoro S., Kennett B.L.N., 2016. Imaging architecture of the Jakarta Basin, Indonesia with transdimensional inversion of seismic noise. Geophys. J. Int., 204, 918-931. https://doi.org/10.1093/gji/ggv466.

Shi X., Zhang S., Jiang M., Pei Y., Qu T., Xu J., Yang C., 2021. Spatial and temporal subsidence characteristics in Wuhan city (China) during 2015-2019 inferred from Sentinel-1 SAR Interferometry. Nat. Hazards Earth Syst. Sci. Discuss., 1-20. https://doi.org/10.5194/nhess-2021-35.

Shirzaei M., Bürgmann R., Fielding E.J., 2017. Applicability of Sentinel-1 Terrain Observation by Progressive Scans multitemporal interferometry for monitoring slow ground motions in the San Francisco Bay Area. Geophys. Res. Lett., 44, 2733-2742. https://doi.org/10.1002/2017GL072663.

Sirait A.M.M., Meltzer A.S., Waldhauser F., Stachnik J.C., Daryono, D., Fatchurochman I., Jatnika J., Sembiring A.S., 2020. Analysis of the 15 december 2017 mw 6.5 and the 23 January 2018 mw 5.9 java earthquakes. Bull. Seismol. Soc. Am. 110, 3050-3063. https://doi.org/10.1785/0120200046.

Tetuko J., Sumantyo S., Member S., Setiadi B., Perissin D., Shimada M., Mathieu P., Urai M., Abidin H.Z., 2016. Giant Sea Wall Using PSI ALOS PALSAR. IEEE Geosci. Remote Sens. Lett., 13, 1472-1476.

Wang C. yuen, Cheng L.H., Chin C. Van, Yu S.B., 2001. Coseismic hydrologic response of an alluvial fan to the 1999 Chi-Chi earthquake, Taiwan. Geology, 29, 831-834. https://doi.org/10.1130/0091-7613(2001)029<0831:CHROAA>2.0.CO;2.

Wessel P., Smith W.H.F., 1998. New, improved version of generic mapping tools released. Eos, Trans. Am. Geophys. Union, 79, 579-579. https://doi.org/10.1029/98eo00426.

Xu X., Sandwell D.T., Smith-Konter B., 2019. Coseismic displacements and surface fractures from sentinel-1 InSAR: 2019 Ridgecrest earthquakes. Seismol. Res. Lett., 91, 1979-1985. https://doi.org/10.1785/0220190275.

Xu X., Sandwell D.T., Tymofyeyeva E., Gonzalez-Ortega A., Tong X., 2017. Tectonic and anthropogenic deformation at the cerro prieto geothermal step-over revealed by sentinel-1A insar. IEEE Trans. Geosci. Remote Sens., 55, 5284-5292. https://doi.org/10.1109/TGRS.2017.2704593.

Yalvac S., 2020. Validating InSAR-SBAS results by means of different GNSS analysis techniques in medium- and high-grade deformation areas. Environ. Monit. Assess., 192. https://doi.org/10.1007/s10661-019-8009-8.

Yang C., Han B., Zhao C., Du J., Zhang D., Zhu S., 2019. Co- and post-seismic deformation mechanisms of the MW 7.3 Iran earthquake (2017) revealed by Sentinel-1 InSAR observations. Remote Sens., 11, 1-17. https://doi.org/10.3390/rs11040418.

Zhang X., Zhang H., Wang C., Tang Y., Zhang B., Wu F., Wang J., Zhang Z., 2019. Time-series InSAR monitoring of permafrost freeze-thaw seasonal displacement over Qinghai-Tibetan Plateau using sentinel-1 data. Remote Sens., 11. https://doi.org/10.3390/rs11091000.

1